Multiwavelength observations of N 66 in the SMC: unveiling photodissociation interfaces and star formation[*]

M. Rubio[1], A. Contursi[2,3,4], J. Lequeux[4], R. Probst[5], R. Barbá[6], F. Boulanger[7], D. Cesarsky[7,9], and R. Maoli[8,4]

[1] Departamento de Astronomía, Universidad de Chile, Casilla 36-D, Santiago, Chile
[2] IPAC, Caltech, MS 100–22, Pasadena, CA 91125, USA
[3] SAp/DAPNIA/DSM, CEA-Saclay, 91191 Gif sur Yvette CEDEX, France
[4] DEMIRM, Observatoire de Paris, 61 Avenue de l'Observatoire, 75014 Paris, France
[5] Cerro Tololo Inter-American Observatory, NOAO, Casilla 603, La Serena, Chile
[6] Facultad de Ciencias Astronómicas y Geofísicas, Universidad Nacional de La Plata, Paseo del Bosque s/n, 1900 La Plata, Argentina
[7] Institut d'Astrophysique Spatiale, Bat. 121, Université Paris XI, 91450 Orsay CEDEX, France
[8] Institut d'Astrophysique, 98 bis Boulevard Arago, 75014 Paris, France
[9] Max-Planck-Institut für Extraterrestrische Physik, P.O. Box 1603, 85740 Garching, Germany

Abstract. We present new observations of the major star–forming region N 66 in the Small Magellanic Cloud and of its surroundings, which add to those presented in Contursi et al. (2000, Paper I). High–sensitivity CO observations allowed the detection of molecular gas associated with the H II region, for which a high–resolution image in [O III] λ 5007 is presented. We also present images in the v(1-0) S(1) line of H_2 at 2.12 μm and in the adjacent continuum. This material reveals an interesting photodissociation region. We show that the molecular gas that has not yet been photodissociated by the UV radiation of the stars is in hot, dense clumps with a very small surface filling factor. We discovered several embedded stars or stellar associations, and suggest that three successive stellar generations have already taken place in less than 3 million years.

Key words: ISM: individual objects: N 66(SMC) – ISM: H II regions – ISM: dust, extinction – galaxies: Magellanic Clouds – infrared: ISM: continuum – infrared: ISM: lines and bands

1. Introduction

N 66 (Henize 1956) is the largest and most luminous H II region in the Small Magellanic Cloud (SMC). It is also known as DEM S103 (Davies et al. 1976) or NGC 346; the latter designates indifferently the H II region and its ionizing cluster. A bright emission region (that we will call N 66 in what follows)

is along and to the SW of an oblique (SE–NW) "bar" (Fig. 1). The H II region is limited on the SW side by a well–defined arc. A more compact H II region at α(J2000)=00h 59m 16s, δ(J2000)=–72° 10′ is N 66A. A supernova remnant is located to the East of the region. A dense cluster of massive young stars excites N 66, but there are also young stars outside, as the ionizing stars of N 66A. Massey et al. (1989) have performed an extensive study of the stellar content of the region, which contains at least 33 O stars, including 11 of type O6.5 or earlier. 22 of these O stars are contained in the central star cluster, and the others are isolated or in small groups. Fig. 1 is a 60 sec OIII image obtained with EMMI/NTT on December 1995, and extracted from the ESO NTT archive through the ESO Science Archive Facility. The image was reduced using reference files obtained during the same observing run using a Tek 2048×2048 CCD, covering a field of view 9.2′× 8.6′ with a pixel size of 0.27 ″.

N 66 has been observed at many wavelengths. In particular Contursi et al. (2000, hereafter Paper I) have presented and discussed mid–IR spectrophotometric observations of N 66 obtained with the 32×32 pixel ISOCAM camera on board the Infrared Space Observatory (ISO) of the European Space Agency. A 6′×6′ field was mapped in 7 broad-band filters, and the central 3′×3′ have been observed with the Circular Variable Filters (CVFs) as dispersive elements. These observations provided a wealth of data on warm dust, fine-structure lines and Aromatic Infrared Bands (AIBs). Mid–IR emission peaks coincide with the main features of the ionized gas map. Fig. 2 shows the contour map in the ISOCAM LW2 filter (5.0–8.0 μm) which is dominated by the 6.2 and 7.7 μm AIB emission, superimposed on the [O III] image of Fig. 1. CO(2–1) line observations made with the Schottky receiver of the SEST telescope at La Silla were also presented. These relatively low–sensitivity observations showed that N 66 does not contain much molecular gas, except for a small cloud to the NE of the bar.
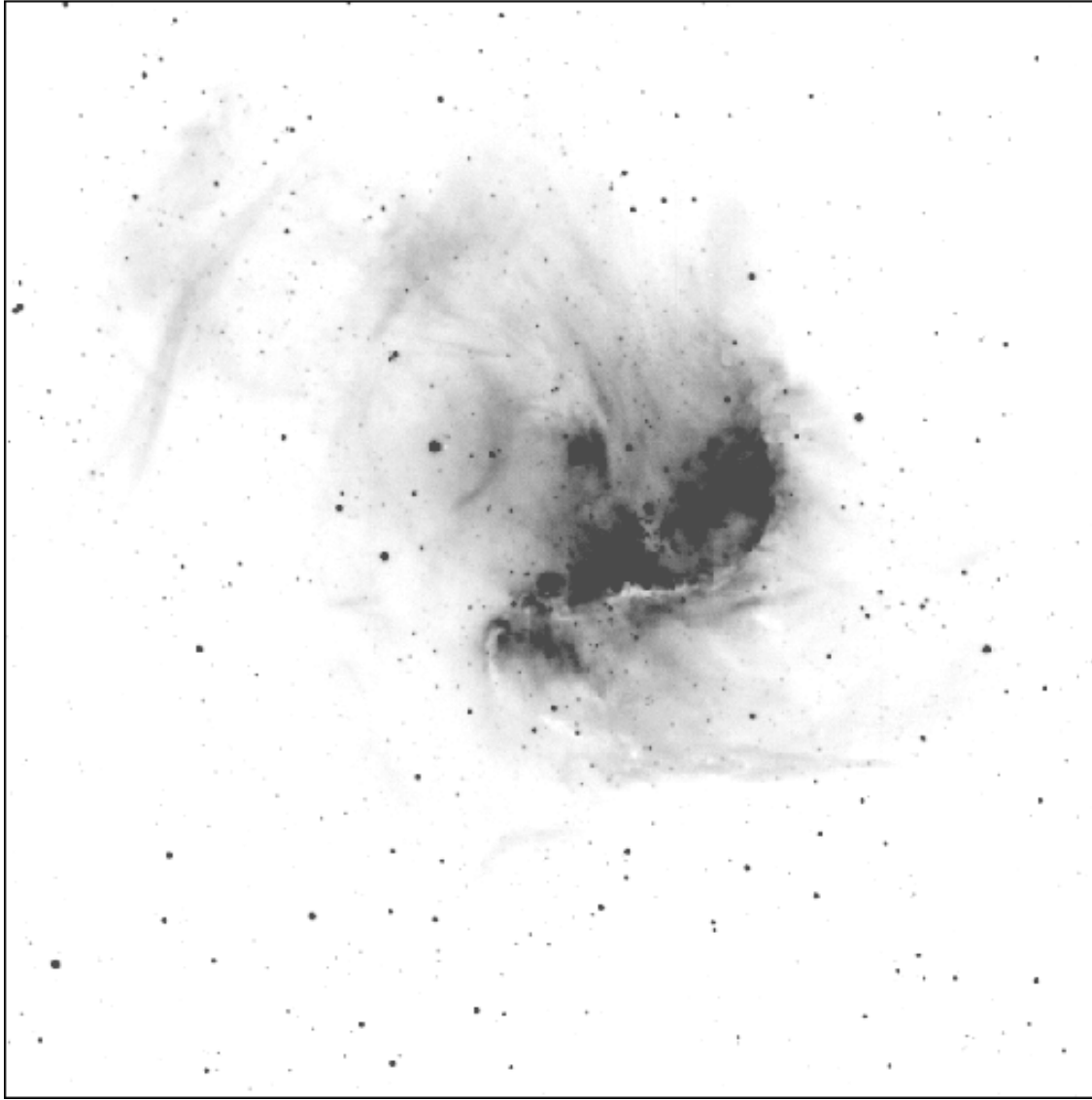
Fig. 1. An archival CCD image of N 66 taken with the New Technology Telescope of ESO through an interference filter centered on the [O III]λ 5007 line. This image displays clearly the structure of the H II region and of its ionizing star cluster, NGC 346. The bright main H II region is limited by a straight boundary on the NE side, probably due to a lack of gas. On the SW side, it is limited by a curved front which is clearly a photodissociation region (PDR) eating into a neutral cloud. Notice the narrow absorption features along this front, that continue to the south forming a S shape. The small H II region N 66A is NE of the main H II region (N 66 proper). The bright star to the East of N 66A is HD 5980, an OB?+WN binary. Other stellar objects in the field are either red supergiants or young OB stars or small clusters. They are identified in Massey et al. (1989) and in Fig. 5 of Paper I. The curved filaments on the top left quarter of the image delineate the supernova remnant SNR 0057-724, which is also a X–ray source (Kahabka et al. 1999).

The present paper describes and discusses new observations of the region of N 66. The CVF observations of the central peak made with ISO are discussed in another paper (Contursi et al. 2000a), with emphasis on the silicate emission. Sect. 2 presents high–sensitivity CO(2–1) line observations made with the SIS receiver of the SEST, which reveal the presence of molecular gas associated with the H II region. In Sect. 3, we present near–IR maps made in the v=(1–0) S(1) line of H_2 and in the adjacent continuum at 2.14 μm. Sect. 4 contains a discussion and Sect. 5 the conclusions.

2. CO observations and data reduction

New CO observations of N 66 have been secured with the SIS receivers of the Swedish–ESO Submillimeter Telescope (SEST) at La Silla during November 1998. These receivers have approximate single–band system temperatures of 400 K and 300 K at 115 and 230 GHz respectively, in T_A^* units. The image band rejections are respectively 20 and 15 dB. In order to convert the T_A^* into main–beam temperatures T_{mb}, one has to divide T_A^* by the main–beam efficiency η_{mb} of 0.70 and 0.60 at 115 and 230 GHz respectively. We performed simultaneous obser-
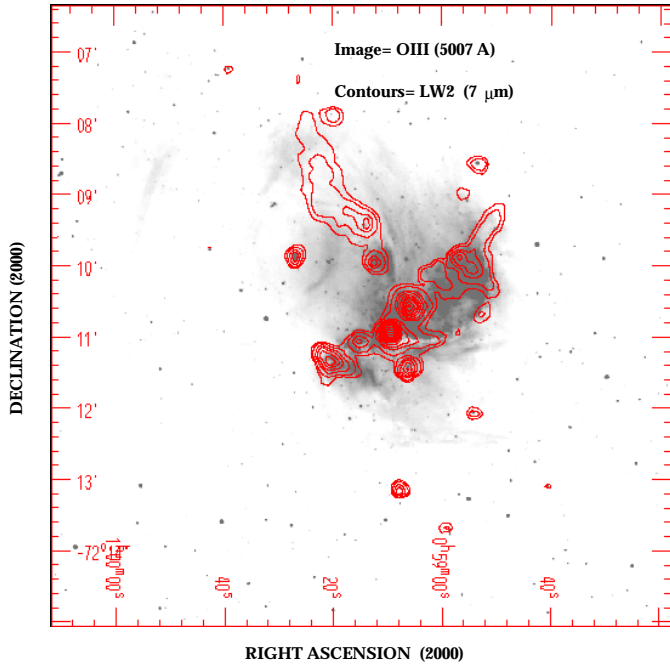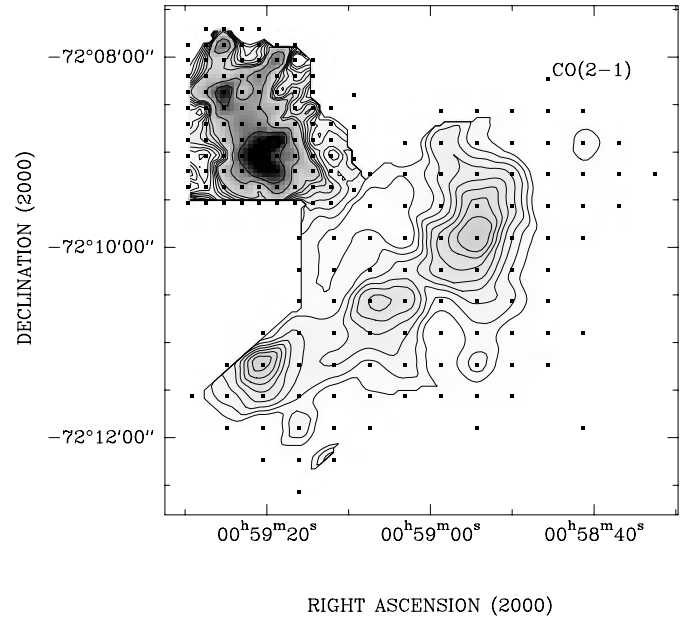
Fig. 2. Contour map in the ISOCAM LW2 filter (5.0–8.0 μm) which is dominated by the 6.2 and 7.7 μm AIB emission, superimposed on the [O III] image. For contour levels and designation of the emission peaks, see Fig. 9. The emission of a number of red supergiants is visible, as well as emission by material close to blue stars or groups of stars (see Paper I). There is mid–IR emission associated with the different H II regions, and with the absorption marks below the main H II region. The mid–IR "spur" to the NE is due to emission by the surface of a molecular cloud (see Fig. 3) visible as an obscuration on the [O III] image.

Fig. 3. Contour map of the integrated CO(2–1) line emission in the region of N 66. The sampling in CO is over a $10'' \times 10''$ grid in the upper left part of the figure, which is built from the old, low–sensitivity SEST observations while the rest of the figure is built from the new, high–sensitivity observations sampled every $20'' \times 20''$. The contours levels are from 0.67 to 3.0 by steps of 0.33, and from 5.0 to 20.0 by steps of 2.5, in units of K km s^{-1}. The temperature scale is T_{mb}. Grid points show the area covered by our old and new observations.

N66 LW2 CO(2−1)

vations in the CO(1–0) and CO(2–1) emission lines over the ionized region. The map was done in the beam–switching observing mode with a $20'' \times 20''$ spacing. The velocity resolution was 0.13 km s^{-1} and 0.056 km s^{-1} per channel at 115 GHz and 230 GHz, respectively. The integration time was 4 min per map position. The rms noise achieved in a single channel was 0.1 K at both frequencies.
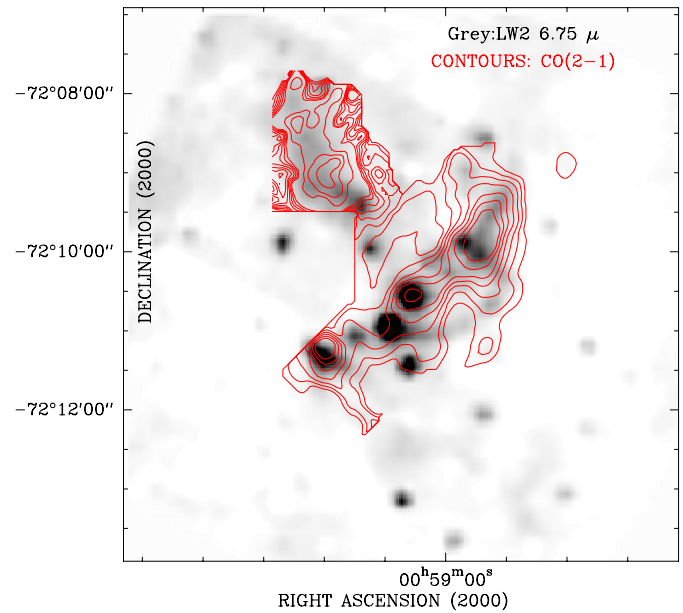
For these observations, we concentrated on sensitivity and due to the limited amount of observing time the region was sampled every $20''$ instead of $10''$ as in the previous observations. The map is thus undersampled given the HPBW of $23''$ of the SEST at 230 GHz. However the sensitivity permitted the detection of CO over most of N 66 where nothing was detected with the older receiver set–up. The Key Programme CO observations towards N 66 were done in CO(1-0) and they covered a $9' \times 9'$ area with a $60''$ grid spacing. CO was detected only in two positions and this emission was fully mapped in CO(1-0) and CO(2-1) as reported in Rubio et al. 1996.

Fig. 3 shows a contour map of the integrated CO(2–1) line. For building this map and the following ones, we have combined the old observations of the molecular cloud in the NE (Paper I) with the new observations. Fig. 4 displays the contours of the integrated CO(2–1) line superimposed over the map in the ISO-

Fig. 4. Contour map of the integrated CO(2–1) line emission in the region of N 66, superimposed over the map in the ISOCAM LW2 filter (5.0-8.0 μm). Contour levels as for Fig. 3. For designation of the peaks of mid–IR emission, see Fig. 8.

Table 1. Parameters of the CO(2–1) line in the direction of peaks identified in Fig. 8. The temperature scale is T_{mb}.

Peak	LSR vel. km s^{-1}	FWHM km s^{-1}	Area K km s^{-1}	Peak intensity K	Remarks
C	160.5(0.1)	3.2(0.1)	1.73(0.03)	0.50	1st component
C	156.9(0.1)	2.8(0.2)	0.60(0.03)	0.20	2d component
D	144.7(0.2)	4.8(0.4)	0.79(0.05)	0.13	
E	145.6(0.1)	3.8(0.2)	1.31(0.05)	0.32	1st component
E	160.9(0.2)	6.0(0.5)	0.92(0.05)	0.14	2d component
	161.9(0.2)	7.2(0.4)	0.99(0.05)	0.13	
G	159.9(0.1)	3.6(0.1)	2.25(0.05)	0.59	
H	145.8(0.1)	3.8(0.3)	0.75(0.05)	0.19	
I	152.0(0.1)	4.2(0.1)	2.72(0.05)	0.61	

CAM LW2 filter (5.0-8.0 μm). There is an excellent correlation between the CO and AIB emissions.

Fig. 5 displays channel maps of the CO(2–1) emission every 5 km s^{-1}, also superimposed over the LW2 filter image (5.0–8.0 μm), smoothed to the 20″ CO resolution. These maps show that the strong emission to the NE is limited to the V_{LSR} range 155–165 km s^{-1}, while the emission associated with N 66 extends from 140 to 165 km s^{-1}, with a complex velocity structure. The CO emission towards the HII region which is seen in the same velocity range as the NE cloud, is clearly spatially separated. Thus, there is no connection between these emissions, and there is no reason to believe that they are physically associated.

Table 1 presents the parameters of the CO(2–1) line in the direction of the well–defined, apparently unresolved peaks identified on Fig. 8. They were obtained by gaussian fitting of the line profile. Due to the incomplete sampling, the true intensity can be somewhat larger, and the data in this table are indicative only.

3. Near–infrared observations and data reduction

Near–infrared observations of the region of N 66 were secured with NICMOS cameras at Cerro Tololo and Las Campanas observatories. The Cerro Tololo observations were obtained at the 1.5m telescope with the 256×256 NICMOSIII infrared camera CIRIM during December 1997. These images were made through narrow filters centered on the v=(1–0) S(1) line of H$_2$ at 2.12 μm and through a similar continuum filter centered at 2.14 μm. This combination provides a continuum subtracted H$_2$ image with limited stellar contamination. Individual images have a field size of 5′×5′ and a scale of 1.16 arcsec/pixel. The total integration time was 2000 seconds on-source for each of the 2.12 μm and the 2.14 μm data sets.

In each filter, individual images were sky subtracted and flatfielded, then combined by median averaging, using IRAF routines. To produce an image with only the molecular gas emission, the 2.14 μm continuum image was scaled to the 2.12 μm image by equalizing the average flux of bright stars away from the field center. Differences in the stellar psf's between the two images, due to seeing, tracking, and slight focus errors were partially adjusted by an 0.5 pixel gaussian smoothing of the

2.12 μm image. Small focus changes with CIRIM produce aberrated images which have no readily modelled dependence on field position. The resulting 2.12 μm continuum-subtracted image is shown in Fig. 6. Bright stars exhibit residual improperly cancelled flux at the 2 percent level due to slight psf mismatches.

Broad band J, H and Ks images of the molecular cloud to the NE of the N 66 HII region were made at Cerro Tololo using the 1.5m telescope with CIRIM in two observing runs (1995 and 1996). The observations covered a 2.5′×2.5′ area with a resolution of 0.64 arcsec/pixel. We have also obtained in November 1997 at the Las Campanas Observatory J, H and Ks images of the mid–IR peaks of emission described in Paper I. These observations were performed with the 256×256 NICMOSIII IR camera IRCAM attached to the 2.5m Dupont telescope. They cover a 1.5′×1.5′ field with a resolution of 0.35 arcsec/pixel. These images will be discussed in a future paper. Here, we have only looked at them qualitatively in order to find embedded stars.

Figs. 6 and 7 show the H$_2$ and 2.14 μm continuum images respectively. The continuum image is dominated by the emission of the exciting stars, with some contribution of field stars. A number of embedded stars which are not or only barely visible optically can also be seen on this image. They have been confirmed by examination of the J, H and Ks images. They are located in Peaks C, D, E, I, and in the compact mid–IR source at the northern tip of the spur as shown in Fig. 7. Also, fainter IR sources are found towards peaks B, H and F.

The H$_2$ image shows a filamentary structure. The filaments to the S-W form an arc which coincides perfectly with the absorption lanes seen on Fig. 1. They also coincide with the emission of the AIBs between 5.0 and 8.0 μm mapped with ISOCAM in the LW2 filter, as shown by Fig. 8. This is characteristic of a photodissociation region (PDR) that is obviously seen edge–on in the present case. Fig. 8 also demonstrates the excellent general correlation between the v=(1–0) S(1) line of H$_2$ and the AIBs. Fig. 10 displays the relation between the H$_2$ line and the CO line, which is also very well marked.

4. Molecular gas and photodissociation regions

A photodissociation region (PDR) develops at the surface of a molecular medium illuminated by FUV radiation. In the PDR,

N66 CO(2−1)
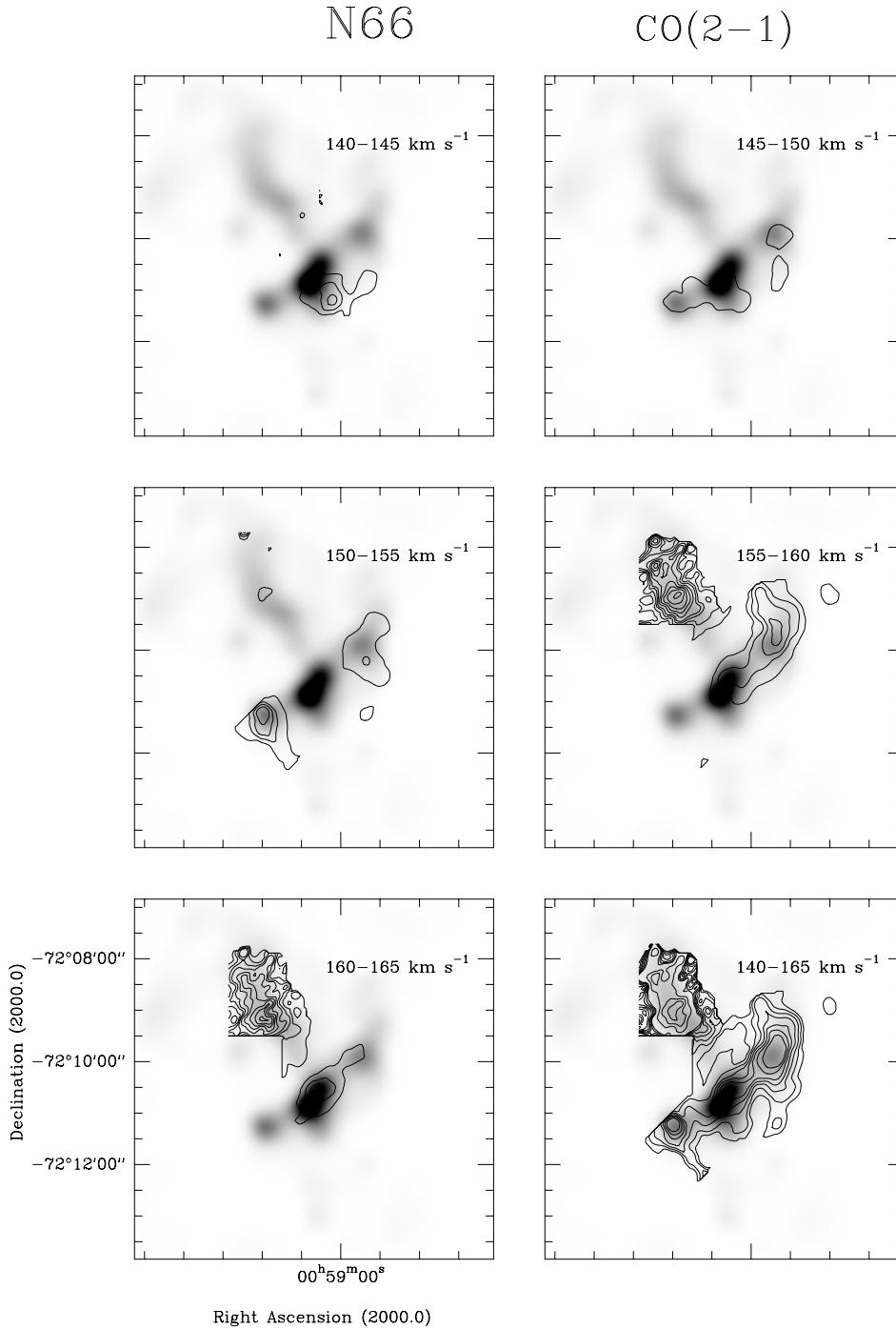
Fig. 5. Contour maps of the CO(2–1) line emission in the region of N 66, in velocity channels 5 km s^{-1} wide, superimposed over the map in the ISOCAM LW2 filter (5.0–8.0 μm), smoothed to a resolution of 20$''$. The LSR velocity range is indicated on each map. For the channel maps, the contours are from 0.42 (3 σ) to 1.67 by steps of 0.42, then from 2.5 to 8.33 by steps of 0.83, in units of K km s^{-1}. The temperature scale is T_{mb}. For the map of total CO (140–165 km s^{-1}) in the bottom right, see the caption of Fig. 3.

molecular hydrogen is partly photodissociated and partly experiences fluorescent excitation, with consecutive emission of vibrational-rotational lines in the near-IR and of rotation lines in the mid-IR. H$_2$ can also be excited collisionally if the density is sufficient, thus the physics of the infrared line emission is complex and diagnosis require spectroscopic observation of line strengths (see e.g. Sternberg & Neufeld 1999 and references herein). The multi–line study of Pak et al. (1998) suggests that the H$_2$ emission is UV–excited in several regions of the LMC whose properties are not too different from those of N 66. CO

like H$_2$ is photodissociated through absorption in UV lines and is self–shielded against photodissociation by the optical thickness in these lines. But CO is more easily photodissociated than H$_2$ and exists only somewhat deeper into the cloud, typically in regions with a visual extinction larger than 1 magnitude compared to 0.1 mag. or less for the v=(1–0) S(1) line of H$_2$. Their respective line emission comes mainly from these depths (see e.g. Lequeux et al. 1994 for examples related to the SMC). The mid–IR Aromatic Infrared Bands (AIBs) and the continuum emission of the Very Small Grains discussed in Paper I are also
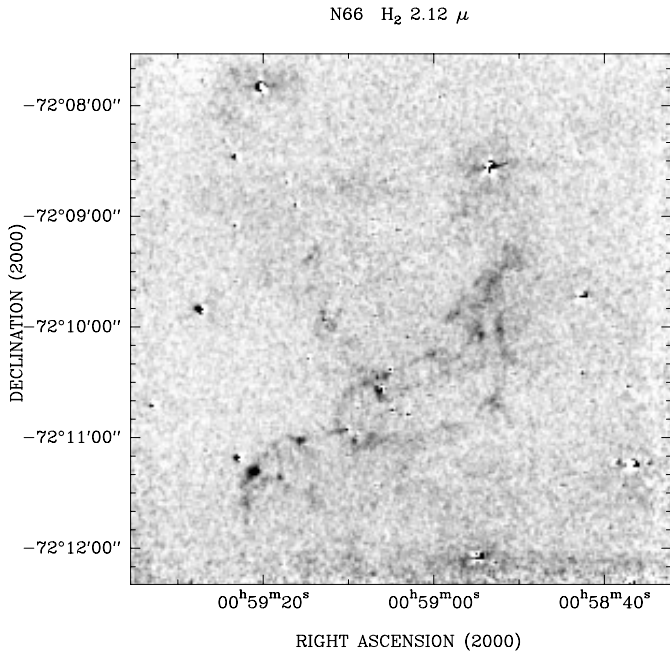
Fig. 6. Continuum–subtracted image of N 66 in the v=(1–0) S(1) line of H_2 at 2.12 μm, obtained at Cerro Tololo. The pixel size is 1.16 arc second.

Fig. 7. Continuum image of N 66 in the continuum at 2.14 μm obtained at Cerro Tololo. The pixel size is 1.16 arc second. The embedded stars or star clusters are designated by numbers, together with the designation of the peaks to which they belong (see Fig. 8 for identification of the peaks).

strongly emitted in the PDR, simply because the matter density increases strongly when entering the front while there is still a large, relatively unabsorbed radiation flux to heat them through absorption of single photons. Thus we expect a strong correlation between H_2 line, CO line and mid–IR emission. This is what is observed in N 66 as illustrated by Fig. 4, 5, 8 and 9. It is interesting to see that even in Peak C, which coincides with the main star cluster with its enormous and very hard ionizing flux, there is still some molecular hydrogen seen in that direction.

The detection of weak CO emission shows that CO has survived photodissociation in the whole region. A similar situation has been observed in the giant HII region 30 Doradus in the LMC (see Rubio et al. 1998, Rubio 1999). In this region, H_2 knots and filaments have been detected associated to cold molecular gas as seen in CO(2-1) emission, surviving from the strong radiation flux of a dense cluster containing more than 60 O stars, as well the strong winds from these stars. Pak et al. (1998) has found a similar situation in several other regions of the Magellanic Clouds. However the high intensity of the [C II] 158 μm line in the same regions and in N 66 (Israël & Maloney 1993) shows that most of the CO has been photodissociated (unfortunately no [C I] line observation seems to exist for the SMC). Pak et al. (1998) assume that the CO lines are optically thick, and explain the observations of the H_2 v=(1–0) S(1), CO and [C II] lines by the emission of uniform spherical clouds immersed in the UV field. There are many such clouds within the observing beam. Each of these clouds is stratified as explained before, with a CO core and a C II envelope. They adjust the cloud radius in order to obtain relative area coverages of the CO cores and C II envelopes such that the ratio between the average surface brightnesses of an ensemble of clouds in the CO and
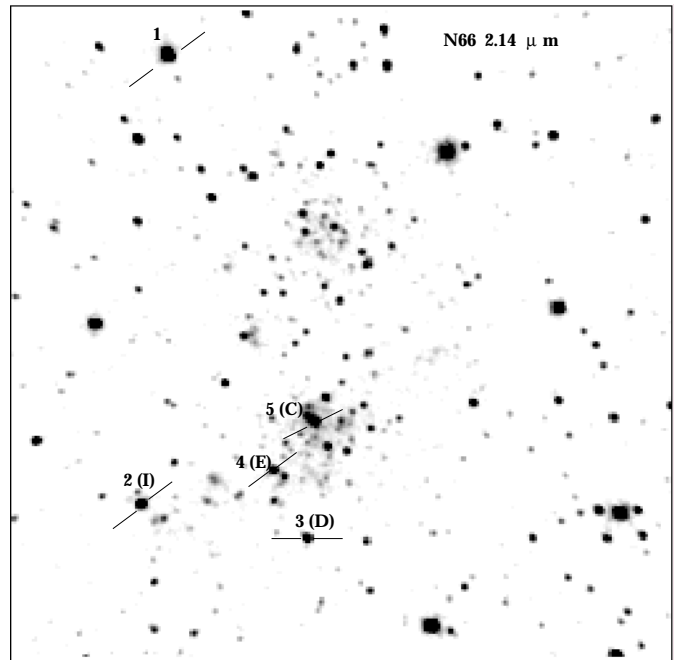
[C II] lines matches the observed line ratio. In this model, an increased UV flux yields a decrease of the size of the CO cores and a corresponding decrease of the CO line intensity. However there is no guarantee that the CO lines are optically thick. Even if they are optically thick, one can imagine many variants such as that proposed by Lequeux et al. (1994) in which the medium is inhomogeneous, with the densest clumps emitting the CO lines and the lower–density regions emitting the [C II] line and a part of the H_2 line. Another possibility is the development of pillars and elephant trunks in the parental molecular cloud by the effect of both the UV radiation flux and the strong stellar winds. The existing observations do not permit a clear choice between these possibilities. Consequently, in this paper, we will limit ourselves to qualitative considerations, and defer to a further paper a quantitative modeling.
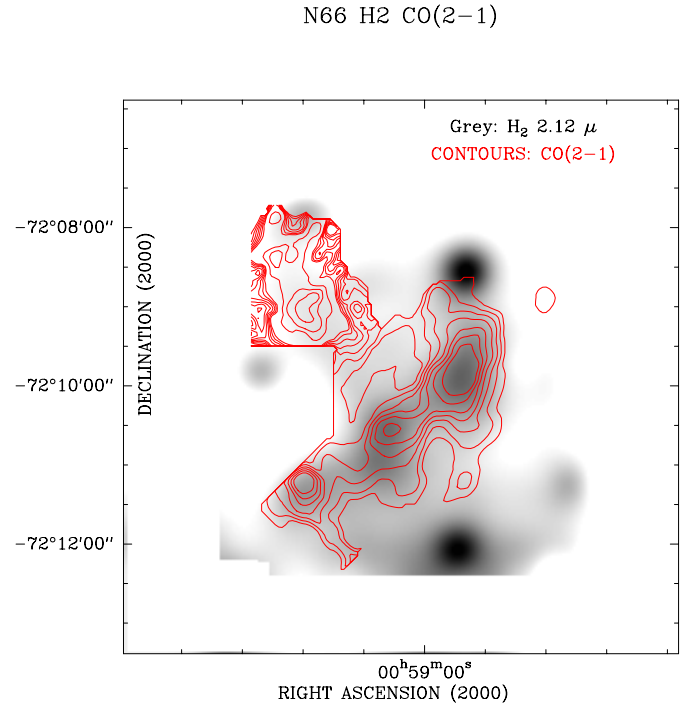
It is unlikely that the CO lines are optically thin because it is difficult to understand how the column density of CO could be adjusted to the small value needed for optical thinness over the large observed spatial extent. Moreover, limits can be set to the density of the CO–emitting medium from the observed intensity ratio of the CO(2–1) and CO(1–0) lines. The CO(2–1)/CO(1–0) line intensity ratio (in units of T_{mb}) is $\simeq$ 1.3 for the emission in the spur, which is adequately sampled in the observations of Paper I. For the rest of the region around N 66 proper, the CO(2–1) observations are not well sampled but it is still possible to have an idea of the global CO(2–1)/CO(1–0) line intensity ratio by integrating the respective emissions over all the map. We find a slightly higher ratio of 1.4. This ratio depends on the
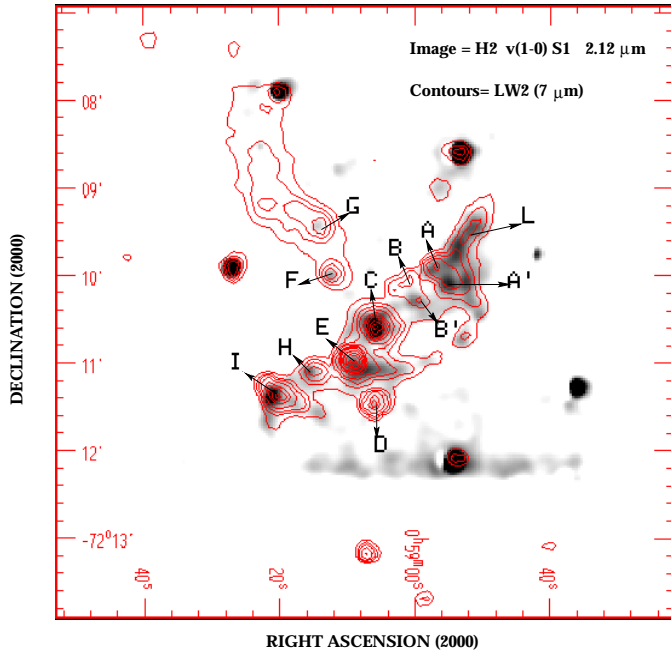
Fig. 8. Contours of the LW2 (5.0–8.0 μm) image of the region of N 66 (resolution $\simeq 6''$) superimposed over the continuum–subtracted image in the v=(1–0) S(1) line of H$_2$ at 2.12 μm smoothed at the same resolution. Contour levels are 0.024, 0.042, 0.059, 0.087, 0.14, 0.17, 0.21, 0.28, 0.35, 0.42 and 0.52 in units of mJy per square arc second. The emission peaks discussed in Paper I are identified by letters.

Fig. 9. Contours of the intensity of the CO(2–1) line integrated over velocity (contour levels as for Fig. 3), superimposed over the continuum–subtracted image in the v=(1–0) S(1) line of H$_2$ at 2.12 μm. This image has been smoothed at the angular resolution of the CO map (20$''$ per pixel).

kinetic temperature, on the density and on the optical depth. Examination of the CO excitation diagrams calculated in the large velocity gradient approximation by Castets et al. (1990, Fig. 16 and 17) shows that in the optically thin case CO(2–1)/CO(1–0) line ratios of 1.3–1.4 require a density larger than 10^3 H_2 molecules cm^{-3} even for kinetic temperatures as large as 100 K in the emitting region. The densities should be even higher in the optically thick case. In the PDRs close to bright H II regions like the Orion ridge, temperature can rise to 100 K and this is probably also the case for a part of the CO–emitting regions in N 66. Even in this case, the density must be larger than 10^3 mol. cm^{-3}.

Presumably the medium is clumpy, and we observe the faint average CO brightness of optically–thick hot clumps with a very small surface filling factor. Given the observed T$_{mb} < 1$ K, the surface filling factor of these clumps is less than 1% instead of $\simeq$ 10% found in less extreme situations in the SMC, as for example in the N 66 spur (Rubio et al. 1993; Lequeux et al. 1994). In the large UV field around the H II regions of N 66, the CO–emitting parts of the clumps have shrunk and the smallest clumps have been completely photodissociated. This reduces the average CO line brightness with respect to the "normal" situation (before the appearance of the hot stars) in spite of an increase of temperature. The contrast between the strong CO emission in the NE spur and the weaker emission in the direction of the H II region can easily be explained in this way, the UV radiation field being considerably smaller around the spur.

One can also explain qualitatively in the same way the observations of the [C II] 158 μm line of Israël & Maloney (1993). This publication contains a contour map of the integrated [C II] line flux obtained with the Kuiper Airborne Observatory with an angular resolution of 55$''$ and a sampling of 40$''$. The reference position of this map appears to be the CO peak. One can recognize the general morphology of the region of N 66, with the bar and the spur. An interesting thing is that the emission of the spur is almost as strong as that of the bar. This confirms that the PDRs in the bar have a small surface filling factor (they are just the surfaces of the molecular clumps), while C II is photoionized into C III as soon as it enters into the H II region. On the other hand, the clumps have a bigger surface coverage in the spur and C II can survive. This compensates for the higher excitation of the line near the H II regions.

We now concentrate on the morphology of the N 66 region. Consider Fig. 5 which displays the CO maps at various velocities superimposed over the smoothed LW2 map. Most of the mid–IR or H$_2$ line emission peaks have a CO counterpart, even Peak C which corresponds to the main ionizing star cluster. Each peak has its own radial velocity, with a possible velocity gradient along the bar. There is also a molecular shell around the main PDR, associated to the velocity range 150–155 km s^{-1}, better seen in the total integrated CO emission (140–165 km s^{-1}) at the lower right panel. Clearly the bar molecular structure existed previously to massive star formation and only a small amount of the initial molecular gas has not been ionized by the central

cluster. Part of the remaining gas is probably pushed by the stellar winds and supernova explosions to form the molecular shell, as the inner side of which we see the PDR tangentially. It is difficult to know if the remaining molecular gas in the bar is located in front or behind the stars formed recently. According to Massey et al. 1989, extinction is small for their stars towards the core (E(B-V)=0.14 on the average), but the interstellar matter is very clumpy and is not likely to produce much extinction even if it lies in front of the stars. In Paper I, we suggested that the formation of the stars which are presently seen optically in N 66 is not coeval. Peak C contains only unreddened stars according to Massey et al. (1989) but Peaks E, H and I for example contain reddened stars suggesting that the interstellar material has not been spread out as much as in Peak C. We proposed in Paper I that star formation along the bar of N 66 has taken place in a sequential way, starting with stars in the more evolved Peak C. This is in agreement with the model and numerical simulations of Elmegreen et al. (1995). The discovery of embedded stars reported in Sect. 3 sheds a new light on this picture. These stars are located in Peaks B, D, E, F, H and I, representing a very recent stellar generation, and there is also an embedded star seen towards Peak C. Whether this star lies within the main stellar cluster NGC 346 or is located behind or in front is not known. It could be that the stars in the core have blown up a cavity in the parental molecular cloud and we see the borders of this cavity delineated by the H_2 emission. Current star formation is thus taking place in the interface region between the ionized and the molecular gas. There is also an embedded massive star (or group of massive stars) at the northern tip of the spur, with associated AIB and H_2 line emission. It indicates a new site of star formation. Curiously, Peak I while quite strong in CO and AIBs is relatively weak in the H_2 line and is not visible in the [C II] line map of Israël & Maloney (1993). Presumably the far–UV flux is still weak in this region.

5. Conclusions

Thanks to a favorable geometry and to the near–absence of foreground extinction and of confusion with other features, N 66 offers one of the best examples of a photodissociation region. We have presented maps in various interesting lines ([O III] $\lambda 5007$, H_2 v=(1–0) S(1), CO(2–1)), of aromatic mid–infrared bands (AIBs) and of continuum at various infrared wavelengths. There is, as predicted by PDR models, a very clear correla-

tion between H_2, the AIBs and CO. We suggest that most of the CO has been photodissociated and that there remains only small molecular clumps with a small area coverage. The CO line emission is thus weaker than in less extreme regions of the SMC because the higher temperature does not compensate for the smaller surface filling factor. We discovered embedded stars (or small unresolved star clusters) in several molecular peaks, which indicate that another stellar generation is starting in this very active region. There are at least three different stellar generations in N 66 within only some 3×10^6 years, the maximum age of the O3 stars. The first generation cannot have started before that time since no Wolf–Rayet star has yet appeared, except for the isolated WR erupting binary HD 5980 whose age is unknown (see Niemela et al. 1999) and the current one, as indicated by the IR embedded sources discovered in our broad band IR survey of the region.

References

Castets A., Duvert G., Dutrey A., et al., 1990, A&A 234, 469
Contursi A., Lequeux J., Cesarsky D., et al., 2000, A&A, submitted
Contursi A., Lequeux J., Cesarsky D. et al. 2000a, in preparation
Davies R.D., Elliott K.H., Meaburn J., 1976, Mem. R. ast. Soc. 81, 89
Elmegreen B.G., Kimura T., Tosa M., 1995, ApJ 451, 675
Henize K.G., 1956, ApJS 2, 315
Israël F.P., Maloney P.R., 1993, in: Baschek B., et al. (eds.), New Aspects of Magellanic Cloud Research. Springer–Verlag, p. 44
Kahabka P., Pietsch W., Filipovic M.D., Haberl F., 1999, A&AS 136, 81
Lequeux J., Le Bourlot J., Pineau des Forêts G., et al., 1994, A&A 292, 371
Massey P., Parker J.W., Garmany C.D., 1989, AJ 98, 1304
Niemela V., Barba R., Morrell N., 1999, New Astronomy Reviews 43, 475
Pak S., Jaffe D.T., van Dishoeck E., Johansson L.E.B., Booth R.S., 1998, ApJ 498, 735
Rubio M., 1999, in: Chu Y., et al. (eds.), IAU Symp 190 "New views of the Magellanic Clouds", ASP Conference Series, p. 67
Rubio M., Garay G., Probst R., 1998, The Messenger 93, 38
Rubio M., Lequeux J., Boulanger F., 1993, A&A 271, 9
Rubio M., Lequeux J., Boulanger F., et al., 1996, A&AS 118, 263
Sternberg A., Neufeld D.A., 1999, ApJ 516, 371